Earth and Planetary Science Letters 325–326 (2012) 63–75

Contents lists available at SciVerse ScienceDirect

Earth and Planetary Science Letters

journal homepage: www.elsevier.com/locate/epsl

Global climate and tectonic controls on the denudation of glaciated mountains

Brian J. Yanites [a,b,*], Todd A. Ehlers [b]

[a] Department of Geological Sciences, University of Michigan, Ann Arbor, 48109-1005, USA
[b] Department of Geosciences, Universität Tübingen, Tübingen, D-72074, Germany

ARTICLE INFO

Article history:
Received 23 June 2011
Received in revised form 27 January 2012
Accepted 28 January 2012
Available online 23 February 2012

Editor: T.M. Harrison

Keywords:
glacial erosion
landscape evolution
erosion rate
climate
Quaternary geology
erosion variability

ABSTRACT

Significant uncertainty exists concerning the efficiency of alpine glacial erosion relative to fluvial and hillslope processes. Latitudinal variations in temperature are important for determining the extent of glaciers, as are the rates of tectonic uplift that influence the elevation (and hence temperatures) that glaciers can form. The acute sensitivity of glacial erosion to temperature has complicated previous interpretations because temperatures must be cool enough to maintain ice yet warm enough to allow glacial sliding. Here we quantify the influence of climate and tectonics on glacial landscape evolution with a coupled glacial, fluvial, and hillslope landscape evolution model that systematically explores variations in rock-uplift rate and periodic variations in climate (i.e. glacial–interglacial periods) over million-year time scales. Emphasis is placed on understanding when a particular climate is either more (e.g. "buzzsaw" conditions) or less erosive than its preglacial landscape. Results indicate that the erosional efficiency of glaciers varies as a function of latitudinal controlled temperature and rock-uplift rate. An order of magnitude increase in erosion rates occurs in some scenarios for both localized (valley bottom) erosion and short-term (one glacial period) durations of glaciation. However, when averaged over the entire landscape for 2 Ma, increases in glacial erosion are typically less than double that of the preglacial landscape. In some scenarios, average glacial erosion rates are less than preglacial rates due to either small, inefficient glaciers or extensive cold-based glaciation. Model predictions are compared with a compilation of long-term denudation rates from glaciated mountain ranges and indicate models perform well at explaining patterns of glacial erosion efficiency. The findings presented here have clear implications for the impact of glaciations on the evolution of landscapes including: (1) the climatic "window" in which glaciers are more erosive compared to pre-glacial rates; (2) spatial and temporal variations in denudation that can lead to pulses of erosion; and (3) predictions of glacial erosional efficiency at different latitudes. We conclude that latitudinal and elevation dependent variations in temperature control the efficiency of glacial denudation and explain discrepancies between previous studies.

1. Introduction

Late Cenozoic cooling and climate variability produced repeated glacial conditions in previously ice-free landscapes. Such changes are hypothesized to increase denudation and limit orogen elevation (Brozović et al., 1997; Mitchell and Montgomery, 2006; Penck, 1905; Porter, 1989). Support for this comes from measurements of glacial sediment fluxes (Hallet et al., 1996) and correlations between topography and snowline altitude (Broecker and Denton, 1989; Egholm et al., 2009). Conversely, although some measurements of long-term denudation rates suggest an increase when glaciation intensifies (Shuster et al., 2005; Valla et al., 2011), denudation magnitudes amongst glacial and fluvial landscapes over long timescales appear similar (Koppes and Montgomery, 2009; Thomson et al., 2010). This discrepancy highlights a fundamental question: Do glaciated landscapes erode faster than unglaciated landscapes?

Three independent lines of evidence suggest glaciers are efficient agents of mountain denudation. First, observations over different timescales document an increase in Late Cenozoic mountain denudation in many glaciated landscapes. This is supported on long time scales (10^5–10^7 yr) from exhumation rates calculated from thermochronology (Berger et al., 2008; Densmore et al., 2007; Ehlers et al., 2006; Fitzgerald et al., 1993; Vernon et al., 2008). On shorter timescales (10^0–10^4 yr) high denudation rates are estimated from sediment fluxes from glaciated catchments (Hallet et al., 1996; Koppes and Hallet, 2006). Second, topographic comparisons between glaciated and nearby unglaciated catchments suggest more efficient erosion by glaciers than by the preceding fluvial system (Brocklehurst and Whipple, 2002). Third, numerical models of glacial landscape evolution reproduce many geomorphic features observed in glaciated landscapes (Egholm et al., 2009; Herman and Braun, 2008; Herman et al., 2011; MacGregor et al., 2000; Pelletier et al., 2010; Tomkin and Braun, 2002) and suggest increased glacial denudation over short and

* Corresponding author at: Department of Geological Sciences, University of Michigan, Ann Arbor, 48109-1005, USA.
E-mail address: yanites@umich.edu (B.J. Yanites).

0012-821X/$ – see front matter © 2012 Elsevier B.V. All rights reserved.
doi:10.1016/j.epsl.2012.01.030

intermediate timescales (10^3–10^5 yr) (Egholm et al., 2009; Tomkin and Braun, 2002) though in some scenarios, numerical modeling predicts decreased denudation rates due to the development of cold-based glaciers (Tomkin and Braun, 2002).

Here we quantify the effects of climate on the evolution of glaciated landscapes undergoing different rates of rock uplift and aim to constrain when a glaciated landscape is more or less erosive than a pure fluvial system. Specifically, we use an orogen-scale coupled precipitation and landscape evolution model (Fig. 1) that incorporates fluvial, hillslope, and glacial processes (Braun and Sambridge, 1997; Braun et al., 1999; Herman and Braun, 2008; Tomkin and Braun, 2002). We simulate the transient response of landscapes to the onset of glaciations to identify what climatic and tectonic scenarios lead to an increase in landscape-wide denudation. We compare these results to characteristics of a number of glaciated landscapes spanning a range of latitudes and rates of tectonic activity (rock-uplift).

2. Methods

2.1. Model set-up

To quantify the effects of climate on glacial landscape evolution over a range of rates in tectonic rock-uplift, we use a modified version of the ICE-Cascade numerical model (Herman and Braun, 2008). There are two main components to the numerical model used in the simulations, a landscape evolution model (Braun and Sambridge, 1997; Herman and Braun, 2008) and an orographic precipitation model (Roe et al., 2003). Within the landscape evolution model, individual modules for fluvial, hillslope (including landsliding), and glacial processes are responsible for eroding, transporting, and depositing material across the model domain (Herman and Braun, 2008; Tomkin and Braun, 2002). Both the fluvial and glacial modules are coupled to an orographic precipitation model that determines both the river discharge based on the precipitation upstream of a point on the landscape and the water equivalent ice input for regions below freezing. The governing equations used in the model are published in the above-cited work and will not be repeated here for brevity.

The general model setup used in each simulation is as follows. A set of user-defined input values are chosen including the tectonically driven rate of rock-uplift, erosional parameters, and climate parameters (Table 1). The initial condition of each landscape is a random (white noise) topography seeded with elevations between 0 and 1 m. Piedmont glacier flow out of the orogen front occurs on a low-sloping continental shelf (slope of 0.001) with no rock-uplift added to edges of this initial landscape. This shelf is added to prevent runaway ice velocities that would otherwise occur if glaciers extended beyond the model domain. The edges of the shelf are held fixed at their initial elevations (i.e. Dirichlet boundary condition). The shelf is not shown in figures (e.g. Figs. 1 and S1) to improve visibility of region where glaciers form. Simulations were run for a total duration of up to 20 My. During this time, sea-level temperature varied as a sinusoid function with a frequency of either 100 or 40 ky and amplitude of 6 °C. Erosion time-steps are variable to ensure model stability and are typically ~10–100 yrs for fluvial and hillslope processes and 0.01 yrs for glacial processes. Note that the terms 'sea-level' and 'base-level' temperatures are used interchangeably hereafter because the elevation of the mountain front is set to 0 m for convenience in interpreting the results. Results from this study can be applied to any orogen so long as the sea/base-level temperature at the base of the orogen is used for comparison.

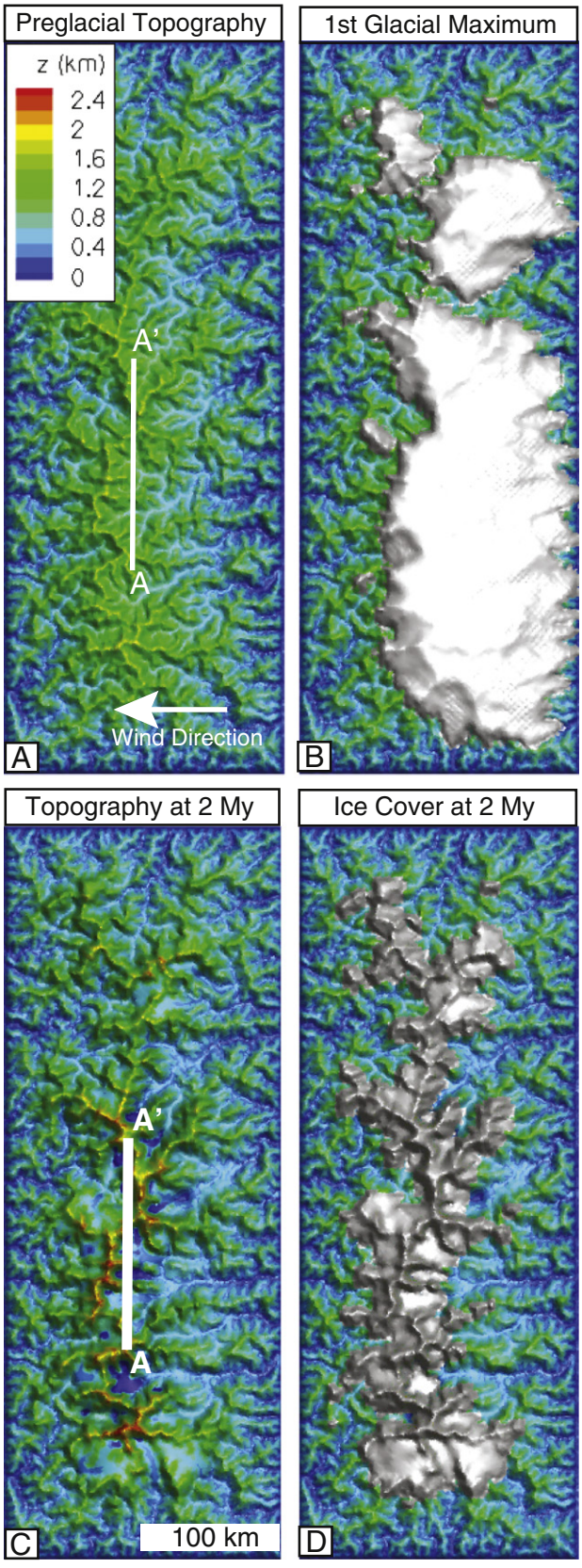

Fig. 1. Modeled topography and ice cover. Shown is both the initial and 2 My topography and ice cover for model run m01 with a rock uplift rate 0.42 mm/yr, glacial sea-level temperature of 2 °C (interglacial 8 °C) and 100 ky glacial–interglacial periodicity. The continental shelf has been removed for illustration clarity. Note the existence of 'buzzsaw' like conditions where glacial extent reduces over time as topography is driven to lower elevation in accumulation zones. Ice cover is shaded in B and D for visualization purposes. Cross-section A–A′ is shown in Fig. 2 and highlights some of the greatest changes to the topography. The strong asymmetry in ice cover in B is the likely the result of not including wind-blown snow transport in the mass balance model.

At each time step, topography of the orogen (but not the shelf) is uplifted based on the user-defined uniform and constant rock-uplift rate across the domain. Flexural-isostatic contributions to rock-uplift due to erosion and ice loads are accounted for. Following rock uplift, the erosion modules update the surface elevations. The rock uplift rates prescribed vary between simulations (Table 1). For the first ~16 My, an equilibrium landscape was produced with only fluvial and hillslope processes (Fig. 1A). For the last 4 My of each simulation, glaciers were allowed to grow and decay in response to climatic oscillations when temperatures are sufficiently cold (Fig. S1, Supplemental material). For regions with greater than 10 m ice thickness, only glacial erosion is allowed to occur (Fig. S1). Sediment entrained by the glacier is immediately passed to the proglacial zone for transport by the fluvial system. In all other regions of the landscape (i.e. with ice <10 m thick) fluvial and hillslope processes operate (Fig. S1).

Model outputs for each simulation are as follows. For each timestep, the topography is calculated at each point on the landscape as a function of the geomorphic processes active. The erosion rates across the landscape are output for each geomorphic process as well as the precipitation (snow or rainfall, temperature), ice thickness, sliding velocity, and the flexural-isostatic adjustment associated with the erosion/ice loads (Fig. S1).

2.2. Climate and erosional process parameterization

Quantifying the role of climate on glacial landscape evolution requires an accurate representation of the spatial distribution of precipitation. To account for this in the model simulations, we use the orographic precipitation model of Roe et al. (2003). This model predicts annual precipitation patterns as a function of temperature, wind speed and direction, and moisture content (Roe et al., 2003). Orographic precipitation was calculated as a function of moisture convergence and temperature variations using the *Clausius–Clapeyron* relationship (Roe et al., 2003) throughout the entire simulation. The temperature and precipitation across the landscape and glaciers is periodically updated (every 5000 yrs) to account for changes in orography due to topographic evolution. Where the temperature is below freezing, the precipitation falls as snow. Snow and ice are melted using a positive-degree day algorithm (Braithwaite, 1995), which is an empirical relationship relating the magnitude of melting to the sum of daily temperatures that are above freezing. The mass balance at a point in the landscape is then calculated by differencing the magnitude of annual snowfall from the orographic precipitation model with the magnitude of potential melting based on the positive-degree day algorithm.

Fluvial erosion is calculated using a linear sediment cover model (Braun and Sambridge, 1997). The function incorporates the local water discharge (calculated with the variable upstream precipitation), sediment supply, local topographic slope, and channel width, which is calculated based on a width-area scaling relationship. Discharge varies in concert with the oscillation of climate conditions on 100 or 40 ky cycles due to the orographic precipitation dependence on temperature (Roe et al., 2003). However, the magnitude of these oscillations is small compared to variability driven process changes associated with glacial–interglacial cycles (see below). Hillslope processes simulated include diffusion and a simple threshold landsliding routine that operates only when hillslopes steepen beyond some user-defined threshold (Burbank et al., 1996; Stolar et al., 2007).

The glacial model assumes a shallow-ice approximation to simulate ice dynamics, modified through a constriction factor (Braun et al., 1999) to account for high-order flow terms due to local topographic effects. Glacial sliding is a function of the driving stresses (Paterson, 1994), and glacial erosion is assumed to be a linear function of sliding velocity (Herman and Braun, 2008). Sliding occurs when the temperature at the ice-bed interface is greater than the pressure adjusted melting point of ice. The ice-bed temperature is calculated with a conductive heat transport model driven by the ice-surface atmospheric temperature and assuming a geothermal heat flux at the base. We added a snow avalanching routine to ICE-Cascade based on the algorithm of Kessler et al. (2006) which assumes a critical slope stability angle (Table 1; Kessler et al., 2006). At every timestep, the snow surface slope between each node and its lowest neighbor is calculated. If the snow surface slope between two nodes exceeds this value (35°), snow is passed from the upper to the lower node. The amount of snow passed is such that the resulting slope will equal the critical stability angle, unless this exceeds the amount of snow present at that node, in which case, 100% of the snow available is moved down slope. Ice that terminates below sea-level on the shelf undergoes iceberg calving, which is assumed to be a function of the depth of ice below sea-level (Paterson, 1994). We keep sea-level constant through these simulations for the simplicity in interpreting model results.

A negative feedback for overdeepening is also included to limit the depth of glacial erosion. The grounding line of a glacier is calculated (i.e. the depth of water needed for ice of a certain thickness to become fully buoyant). This is not intended to represent the effects of subglacial hydrology on basal sliding which is a beyond the scope of this study, but a potentially important, physical aspect of the glacial system (Bartholomaus et al., 2008; Flowers and Clarke, 2002; Herman et al., 2011; Kamb, 1987). Instead, this is to acknowledge the inability for a glacier to erode if it is not in contact with its bed. We assume sea-level as the equipotential ground water surface for simplicity, but note that more rigorous calculations of a hydrologic field could allow this effect to be incorporated at higher altitudes. As an overdeepening erodes below sea-level, we assume that the erosion will decrease as buoyant forces reduce the force exerted at the ice–bedrock interface. The erosion potential of the ice linearly declines as the bed lowers below sea-level as a function of the relative forces of the weight of ice above and the buoyant force exerted by the water below. This allows a gradual transition from a rapidly developing overdeepening to a stable landform. The model parameter is pinned at two values: (1) the value is unity when the ice–bed interface is at sea-level (i.e. no impact on erosion); and (2) the value is zero when the ice becomes fully buoyant and the ice–bed interface is at the grounding line. Note that this erosional reduction value is affected by changes in either ice thickness or the elevation of the ice–bed interface. Thus the maximum depth of an overdeepening is not a predetermined factor as in other studies (Kessler et al., 2008), but rather results from the interaction of climate, topography, and glacial erosion.

2.3. Exploration of model free parameters

A total of 92 simulations were conducted with different climate, rock uplift rates, and erosional parameters (Table 1, Supplemental material). The effects of climate on denudation are explored by varying the sea-level temperature of each simulation from −4 °C to 15 °C during glacial periods (2 to 21 °C during interglacial periods). A 6° C sinusoidal oscillation in temperature occurs in each simulation. For each sea-level temperature simulated (Table 1), we explore a range of tectonically driven rock-uplift rates, which lead to a range of initial landscape relief values, defined as the difference between maximum landscape elevation and baselevel (sea-level for these model simulations). Steady-state rock uplift rates considered are 0.42, 0.84, 1.25, and 2.5 mm/yr. These parameter combinations were run for both 100 ky and 40 ky climate periodicities to test for the control of climate variability on glacial landscape evolution. To test for model sensitivity to erosional parameters the previous combinations of climate and rock-uplift were repeated with a higher glacial erosion coefficient (increased by 10×). The sensitivity of denudation to the fluvial erosion parameter was tested by running the rock-uplift rates of 0.42

Table 1
Landscape evolution and orographic precipitation model parameters.

Variable name/description	Value (range)	Units	Reference
Model set-up			
Dimensions	150×400	km	
Node spacing	1	km	
Tectonic (rock uplift) parameters			
Rock-uplift rate[a]	0.42, 0.84, 1.25, 2.5	mm/yr	
Flexural plate length	1000	km	Braun and Sambridge, 1997
Elastic plate thickness	15	km	Braun and Sambridge, 1997
Young's Modulus	1.00E + 11	Pa	Braun and Sambridge, 1997
Poisson's ratio	0.25	Non-dimensional	Braun and Sambridge, 1997
Density of crust	2750	kg/m^3	Braun and Sambridge, 1997
Density of asthenosphere	3300	kg/m^3	Braun and Sambridge, 1997
Fluvial and hillslope erosion parameters			
Bedrock fluvial eroison coefficient[a]	3.50E-04	Non-dimensional	Braun and Sambridge, 1997
Bedrock erosion length scale	1000	m	Braun and Sambridge, 1997
Channel width scaling coefficient	0.1	$(yr/m)^{0.5}$	
Discharge threshold	4	m km^2/yr	Braun and Sambridge, 1997
Alluvium length scale	100	m	Braun and Sambridge, 1997
Hillslope diffusivity	2 e-6	km^2/yr	Braun and Sambridge, 1997
Threshold hillslope landsliding	30	Degrees	Burbank et al., 1996; Stolar et al., 2007
Climate			
Base-level temperature[a] (glacial)	−4, −2, 0, 2, 4, 6, 9, 15	°C	
Glacial/interglacial temp difference	6	°C	
Periodicity of temperature[a]	[40][100]	ky	
a0	0.3	m/yr	Roe et al., 2003
a1	110	m/yr per (m/s)	Roe et al., 2003
Alf	100	1/(m/s)	Roe et al., 2003
Average wind speed	0.6	m/s	Roe et al., 2003
Wind direction angle from x-axis	90	Degrees	Roe et al., 2003
Glacial erosion parameters			
Ice-flow constant	6.80E-24	$1/(Pa^3\ s)$	Braun et al., 1999
Ice-sliding constant	1.00E-15	(1/((Pa^ice sliding exponent) s))	Braun et al., 1999
Ice-flow exponent	3	Non-dimensional	Braun et al., 1999
Ice-sliding exponent	3	Non-dimensional	Braun et al., 1999
Ice density	910	kg/m^3	Braun et al., 1999
Atmospheric lapse rate	6.5	°C/km	
Constriction constant	1.00E + 03	m	Braun et al., 1999
Calving coefficient	2	1/yr	Kessler et al., 2008
Basal heat flux	5.00E-02	W/m^2	Herman and Braun, 2008
Ice thermal conductivity	2.4	W/mK	Herman and Braun, 2008
Positive degree day melting coefficient	8.00E-03	K m/yr	Braithwaite, 1995
Annual temperature variations	15	°C	
Now stability angle for avalanching	35	Degrees	Kessler et al., 2006
Glacial erosion coefficient[a]	1.00E-03	Non-dimensional	Humphrey and Raymond, 1994

[a] Denotes free parameter explored in simulations presented in this manuscript.

and 0.84 mm/yr suite of model runs with a fluvial erosion coefficient reduced by 50%.

3. Results

3.1. Simulated topography

The modeled topographies reproduce many features that are typical of glaciated landscapes including: hanging valleys, overdeepenings, U-shaped valleys, cirques, and arêtes (Figs. 1 and 2A). Many of these features are apparent in topographic cross sections of the model output (Fig. 2A) suggesting the modeling approach captures the underlying physics of glacial landscape modification. Fig. 2 also highlights that changes in denudation are not spatially uniform in glaciated terrain (Herman and Braun, 2008). For example, a number of valleys see a large increase in denudation, lowering their elevation, whereas some peaks gain topographic elevation as cold-based ice inhibits erosional processes from operating (Fig. 2B). Fig. 2C and d show the instantaneous (a single model time-step of ~3 days) erosion rate across the landscape for the same time slices shown in Fig. 1A and C, respectively. The zone of maximum glacial erosion migrates headward from the mountain front towards the drainage divide as topography evolves due to the glacial processes. This pattern of headward erosion over 2 My is similar to that inferred from thermochronology data in New Zealand (Shuster et al., 2011). We note that measuring localized changes in erosion rate, for example using an age–elevation transect with thermochronology, may not accurately capture the spatial variations in landscape-wide denudation due to glaciation.

Spatial variability in the topographic response to glaciation is also highlighted by changes in the hypsometry of the landscape (Fig. 3). The range of the glacial to interglacial ELA strongly influences what parts of the landscape have increased or decreased denudation rates compare to the pre-glacial landscape. For example, in Fig. 3A ~18% of the initial topography (blue line) is above the interglacial ELA. This large area is perennially covered by cold-based glaciers that inhibits erosion and allows in increase in the elevation of some peaks. At lower elevations, however, large, wet-based glaciers erode faster than the rate of rock-uplift and reduce elevations within and below the range of elevations of the ELA. In Fig. 3B, most of the landscape (~95%) exists at elevations lower than the interglacial (maximum) ELA. This results in glacial erosion that efficiently reshapes topography

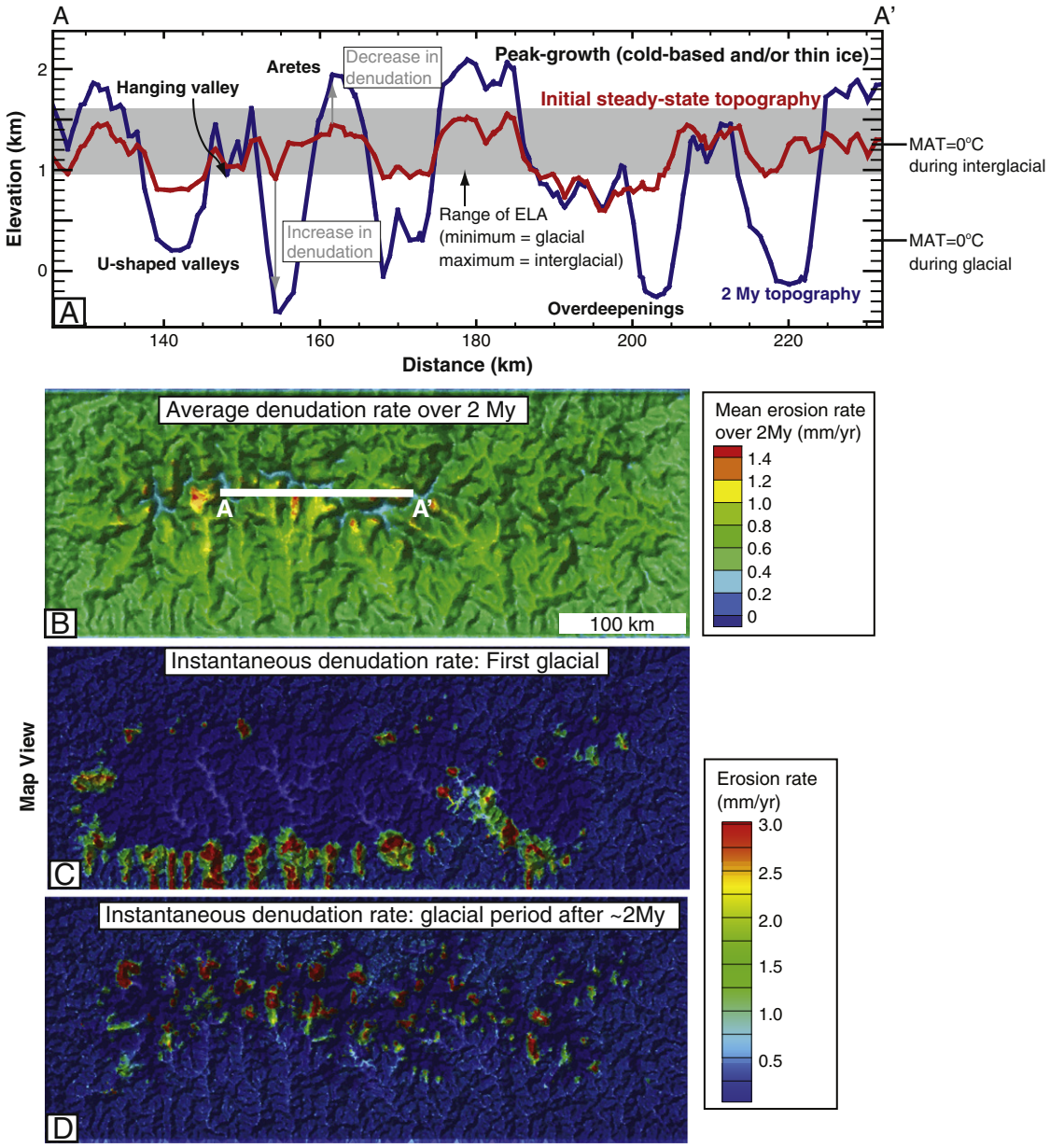

Fig. 2. Spatial variability in denudation. (A)Topographic cross section A–A′ from Fig. 1. Red-line is the pre-glacial steady-state topography. Blue line is the topography 2 My after the onset of glaciation. Note the development of wide, U-Shaped valleys, sharp ridge-lines (i.e. aretes), hanging valleys, and overdeepenings. The cross-section also highlights the spatial variability in denudation following glacial onset. For example, near distance 155 km distance, the landscape eroded more than 1 km of material beyond the back-ground rate of rock-uplift of 0.42 mm/yr (840 m over 2 My), whereas only 5 km further along the transect (distance 160 km), denudation was muted and topography gained elevation. (B) Spatial distribution of mean erosion rates averaged over 2 My following the onset of glaciation. Note the high spatial variability near the headwaters. (C) Rate of denudation during the first glacial period following the onset of glaciation. Notice high rates of denudation are located at the ice margin where the ice is thick and wet-based. (D) Rate of denudation during a glacial period after 2 My of model simulation. Notice the zone of high denudation has propogated in from the mountain front as efficient glacial erosion has limited the accumulation area and extent of ice cover (Fig. 1).

at high elevations. At lower elevations, topography remains fairly undisturbed since glaciers are limited to relatively higher elevations.

3.2. Erosion rate time series

Results indicate that an increase or decrease in landscape-wide denudation rates relative to preglacial rates depends on the local base-level elevation (sea-level in these models) climate as well as the initial landscape relief determined by the rate of rock-uplift and erosional parameters (Whipple and Tucker, 1999). The influence of climate and rock-uplift rate on denudation rates in landscapes influenced by glaciation is large (Fig. 4, see also Supplemental Figs. S2–S5). For example, in Fig. 4A average denudation rates in the glaciated part of the landscape are increased by a factor of ~2 above the background (preglacial) level for approximately 1 My as topography equilibrates to a new (glacial) geomorphic process. Contrary to this, Fig. 4B demonstrates that cooler climates and/or higher rates of rock-uplift decrease denudation rates by generating conditions dominated by cold-based glaciers. We note that localized zones of enhanced erosion do occur in such situations at low elevations where the bed is above freezing and thick ice drives rapid sliding, but the average denudation rate across the glaciated landscape is lower due to the widespread occurrence of cold-based glaciers. Furthermore, we find that the denudation rates of glaciated mountains are highly variable over a range of timescales. Denudation rates and their differences during glacial and interglacial conditions are not constant and

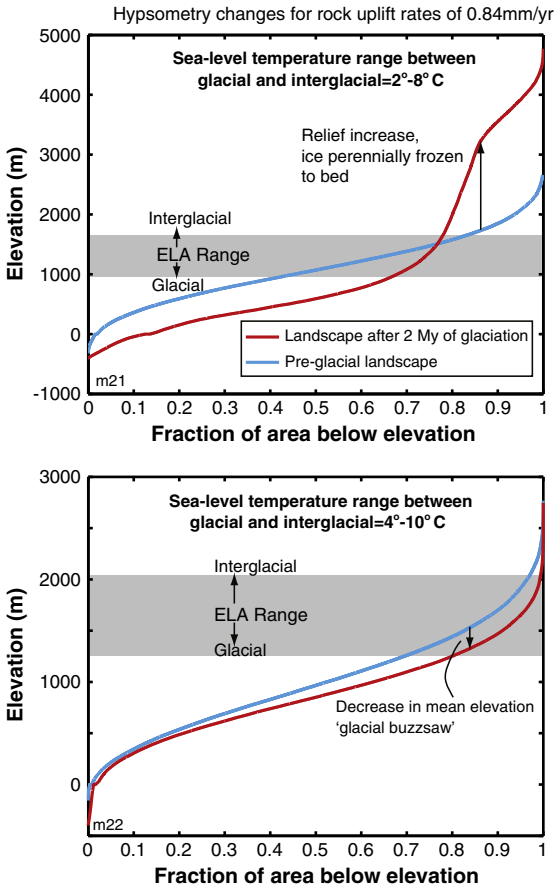

Fig. 3. Hypsometric evolution of modeled landscapes undergoing a rock-uplift rate of 0.84 mm/yr. Each plot shows the pre-glacial landscape in blue and the landscape after 2 My of glacial processes in red. (A) Represents results for a sea-level temperature range of 2–8 °C, and (B) is for a climate 2 °C warmer. Note the shift in the ELA has a strong control on how glacial processes influence the topographic hypsometry.

vary over timescales of 10^3–10^4 yrs. For example, in Fig. 4B, the denudation rate during a glacial maximum at ~3.5 My is a factor of five higher than the interglacial rate immediately before and after this peak. Finally, erosion variability also occurs over timescales of 10^5–10^6 yrs as topography readjusts to the new mean climate state and the hypsometry of the topography evolves in response to glaciation (Fig. 3). Such variability in denudation rates suggests a highly nonlinear response associated with the development of topography and glacial conditions. The high variability in glacial denudation rates (Fig. 4) implies a sometimes unrecognized outcome that denudation rates measured from different techniques are dependent on the time scale of observation (e.g. Koppes and Montgomery, 2009).

A number of processes and their interactions lead to the variable and nonlinear erosion history visible in Fig. 4. For example, as a glacier erodes a valley bottom, the adjacent valley walls increase in slope and enhance the rate of snow avalanching leading to greater valley ice thickness and sliding velocities. This process also exposes hillslopes to erosion thereby enhancing landscape-wide erosion. These combined effects cause increased erosion that lags the onset of glaciation (e.g. 0.9 My, Fig. 4A). The transience continues until topography is sufficiently modified to lower hillslope angles and reduce the rate of erosion. In other scenarios, the spatial distribution of cold-based and wet-based glaciers leads to topographic steepening near the transition between perennial cold-based glaciers and wet-based, erosive glaciers. Because the wet-based region erodes and the cold-based region does not, topography steepens at this transition. Eventually the slope at the transition surpasses the threshold angle of landscape stability and bedrock landslides lead to short pulses of erosion (e.g. at ~3.5 My in Fig. 4B). Another mechanism for the nonlinear erosion histories in Fig. 4 is the breaching of divides by glaciers and the landscape adjustment to the new ice flow paths. As large glaciers fill their valleys with ice, low topographic saddles along the ridges provide a passageway for the transport of ice to adjacent valleys. This redistribution of glacial ice can increase sliding velocities and generate topographic transience across the ridge and in the adjacent valley.

3.3. Evolution of relief

The preglacial steady-state orogen relief (peak elevation minus baselevel elevation) is strongly influenced by the rate of rock-uplift (Fig. 5A). Higher rates of rock-uplift require steeper rivers to erode at the same rate (Whipple and Tucker, 1999) and therefore result in higher topography. Climate plays a secondary role in influencing the preglacial orogen relief (Fig. 5A). Cooler climates result in higher topography for a given rate of rock-uplift. This results from temperature dependent orographic precipitation model (Roe et al., 2003), which generates lower precipitation at the cooler temperatures. The lower precipitation causes a decrease in water discharge and therefore less fluvial erosion capacity. This produces overall higher river channel slopes and orogen-scale relief.

Following the onset of glaciation, the orogen scale relief changes. This evolution is strongly controlled by climate because temperature influences the denudation rate history (Fig. 4) as well as the distribution of cold and wet-based glaciers (Fig. 3). In a cool climate in which cold-based glaciers protect peaks and high altitude topography from erosion, orogen relief grows at roughly the pace of rock-uplift (blue line, Fig. 5B). Variations in flexural-isostatic adjustment as well as large landslides (Burbank et al., 1996) can cause deviations from this trend. In warmer climates, wet-based glaciers lead to a more complex relief evolution. For example, for a rock-uplift rate of 0.84 mm/yr and a baselevel interglacial temperature of 10 °C, relief initially increases following the onset of glaciation (black line, Fig. 5B). After ~1 My, the rapid erosion in the valleys has sufficiently steepened the adjacent hillslopes, and the erosion propagates upslope, primarily through landslides, and peaks are lowered. In an even warmer climate (red line, Fig. 5B), the lag between valley erosion and peak lowering is extended as the smaller, less efficient glaciers take more time to steepen the adjacent hillslopes. Because landscape dynamics are highly variable in these systems (Figs. 4 and 5B), we focus in the following sections on denudation rates averaged over 2 My to provide a measure of the long-term efficiency of the glacial system.

3.4. Long-term (million year) changes in erosion rate

In this section we highlight the sensitivity of orogen glacial denudation rates to changes in the baselevel (sea-level in these examples) temperature and rock uplift rates. Denudation histories are sensitive to changes in both of these parameters. We isolate each variable in Fig. 6 to demonstrate the general behavior of these two parameters before presenting the effects for a wider range of climate and rock-uplift rates (Fig. 7).

Glacial denudation rates demonstrate large sensitivity to variations in the rock-uplift rate for two different baselevel temperatures (Fig. 6A). For a low rock-uplift rate (0.42 mm/yr), a relatively warm climate (10 °C during the interglacial in Fig. 6A) will generate very limited ice cover and only small, inefficient glaciers. Analysis of model results indicates this is because the maximum elevation is low (1730 m) and the ELA barely dips below the peak elevations during glacial periods. This results in a period of decreased erosion and an over all reduction in the average denudation for portions of the

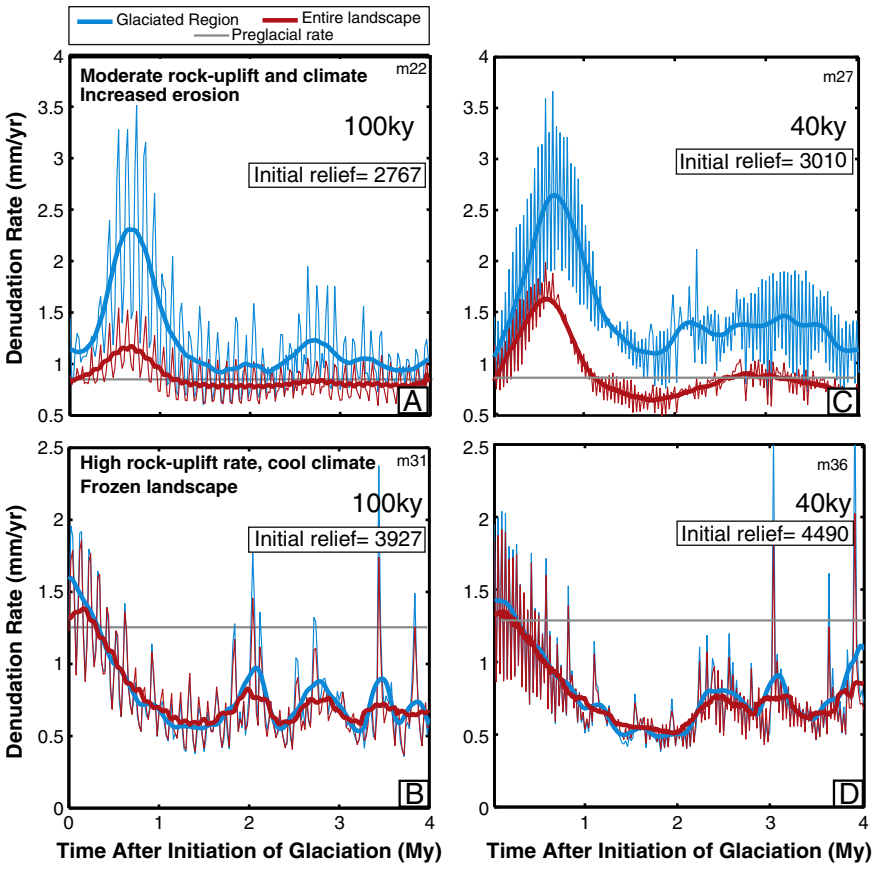

Fig. 4. Erosion histories for two simulations with different tectonic rock uplift rates and climates. Panels highlight the temporal variability in denudation rate of mountains experiencing a 100 ky (A–B) and 40 ky (C–D) variation in climate between glacial–interglacial conditions. Bold, blue lines show running 200 ky denudation rate averages, lightweight, blue lines show 10 ky averages. Red lines indicate denudation rates in non-glacial portions of the landscape where ice thickness is <10 m, gray lines are the average denudation rates in the pre-glacial landscape at steady-state. (A) Simulation m22 (rock uplift = 0.5 mm/yr, glacial sea-level temperature 4 °C) also shows an increase in denudation. (B) Simulation m31 shows decreased denudation due to the 'freezing in' of peaks (mean and max elevation of 1072 and 3123 m respectively; rock uplift = 1.25 mm/yr; glacial sea-level temperature at lowest elevation = 2 °C). (C) Simulation m27 is the same as m22 (A) but with a 40 ky climate periodicity. (D) Simulation m36 is the same as m31 (B) but with a 40 ky climate periodicity. Results for other rock uplift rates are available in the supplementary material.

landscape influenced by the small glaciers. A higher rate of rock-uplift at the same base-elevation temperatures (0.84 mm/yr, 10 °C) generates a higher peak elevation (2767 m) (Fig. 6A). This results in larger glaciers that are capable of eroding rapidly and increases the denudation rates for the glaciated portions of the landscape (Fig. 6A). However, denudation rates do not continue to increase as the rate of rock-uplift increases. The highest elevation (5511 m) is generated with a 10 °C climate and a rock-uplift rate of 2.5 mm/yr. These higher elevations result in a landscape covered by extensive cold-based glaciers that act to reduce the average denudation rate (Fig. 6A). In contrast to the previous change in denudation rates shown for a 10 °C climate, denudation rates are higher in a slightly cooler climate (8 °C) with a rock-uplift rate of 0.42 mm/yr (Fig. 6A). Denudation rates are higher in this cooler (8 °C) climate because greater ice cover develops and produces erosive warm-based glaciers. However, the change in denudation rates decreases in this cooler climate at higher (>0.84 mm/yr) rock-uplift rates due to the development of higher elevation and more cold-based glaciers. Finally, comparison of results for a single rate of rock-uplift (1.5 mm/yr) and two climates (8 and 10 °C, Fig. 6A) is also informative. The landscape in the cooler climate, experiences lower denudation following the onset of glaciation (Fig. 6A) due to cold-based glaciers; however, a warmer climate produces increased denudation rates because a higher-proportion of the glaciated landscaped is covered by erosive wet-based glaciers than the cooler climate.

Variations in denudation rates from different interglacial baselevel temperatures are also significant (Fig. 6B). For example, at the lowest rate of rock uplift (0.42 mm/yr, Fig. 6B) the maximum enhancement in denudation occurs at ~6 °C whereas below 4 °C and above 8 °C denudation rates are lower than the preglacial landscape. A base-elevation temperature of 8 °C is predicted to increase denudation averaged over 2 My for rock-uplift rates of 0.42 and 0.84 mm/yr, which produce initial relief of 1.8 km and 2.9 km (Fig. 6B). However, denudation rates decrease below preglacial levels for rock-uplift rates of 1.25 and 2.5 mm/yr. These higher rates of rock-uplift produce initial relief of 3.9 and 6.3 km and consequently much cooler temperatures that lead to cold-based glaciers at these higher elevations. These higher rates of rock-uplift require warmer baselevel temperatures to produce wet-based glaciers to increase denudation above preglacial levels (Fig. 6B).

We find that the boundaries separating decreased and increased denudation are described by a simple measure of the temperature distribution over a mountain range (Fig. 6C). More specifically, the percent of the landscape with a mean annual temperature (MAT) below freezing during the interglacial defines two thresholds for when climate, via glacial denudation, imprints topography (Fig. 6C). For example, a decrease in denudation rates relative to preglacial conditions occurs when either less than ~5–10% or greater than ~60–80% of the landscape is below freezing (Fig. 6C). Between these values, denudation rates increase (Fig. 6C). These values define the transition

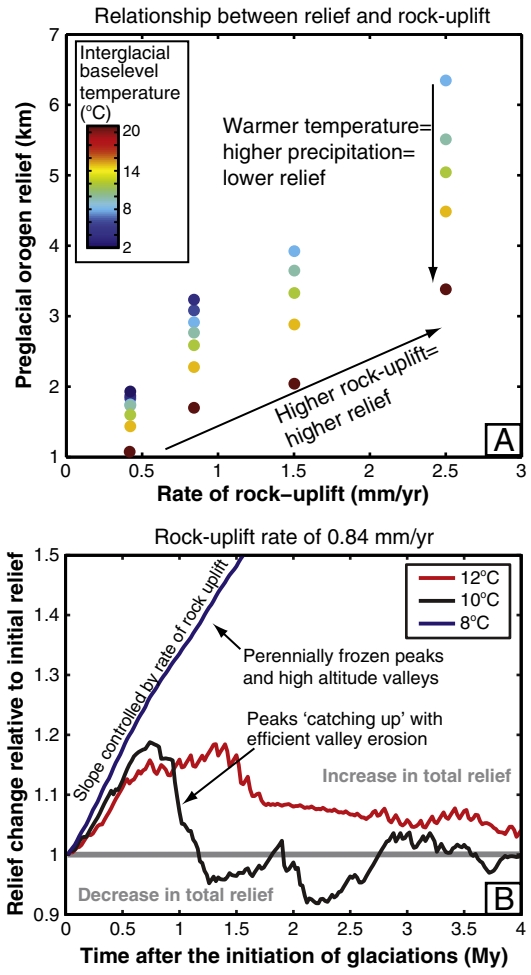

Fig. 5. The influence of rock-uplift rate on orogen relief for different climates. Symbol color denotes the baselevel (sea-level) interglacial temperature. The range of relief for a given rate of rock-uplift is a result of the temperature dependent *Clausius–Clapeyron* relationship in the orographic precipitation model, such that warmer temperatures generate greater precipitation at high altitudes, which lowers overall orogen relief. (B) Evolution of relief relative to initial relief for three runs with the same rock-uplift rate (0.84 mm/yr) but different climates (8, 10, and 12 °C). For the coolest climate (8 °C), relief grows at the rate of rock uplift due to perennially frozen peaks and high altitude landscape. At warmer temperatures, wet-based glaciations allow for enhanced erosion that prevents relief growth.

from small, headwater glaciers to large, erosive valley glaciers (5–10%); and from erosive, wet-based glaciers to unerosive, cold-based glaciers (60–90%).

The previous results highlight that different rates of rock uplift produce different magnitudes of topographic relief (Fig. 5A). Keeping this in mind, it is insightful to examine changes in the glaciated landscape denudation rates as a function of both the base elevation temperature and orogen relief (Fig. 7). The results identify a climatic "window" where an increase in denudation due to glaciation can be expected for a given magnitude of relief (Fig. 7A). The "window" (gray zone) expands at higher relief values, such that a broader range of baselevel climates are expected to increase denudation for higher topographies. Furthermore, the temperatures that define the window increase with increasing topography and rock-uplift (Fig. 7A). This occurs because the temperature must be cool enough

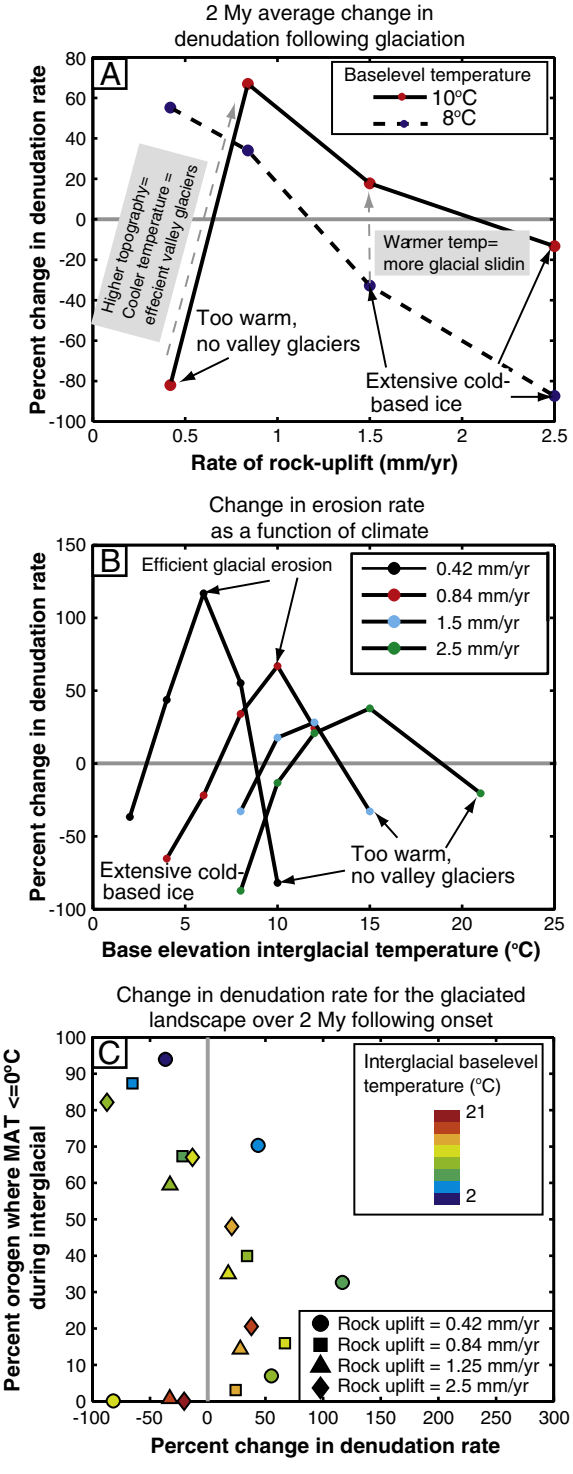

Fig. 6. (A) Variations in the percent change in denudation rate (relative to preglacial rates) as a function of rock-uplift rate. Results are shown for two different interglacial baselevel climates. For the cooler climate (8 °C), the greatest percent change in erosion occurs for the lowest rock-uplift rate (and lowest initial relief). With increasing rock-uplift rate (and higher initial topography), the expansion of cold-based glaciers limits glacial erosion. For a warmer climate (10 °C), the lowest rock-uplift rate has reduced erosion because of shallow ice cover that does not develop large valley going glaciers. Higher topography (from higher rock uplift) allows greater ice accumulation and the development of valley glaciers that efficiently erode the landscape. (B) Percent change in denudation rate versus climate for each set of rock-uplift runs. For a given rate of rock-uplift, the greatest increase in glacial erosion occurs at a moderate temperature. In cooler climates, extensive cold-based glaciation limits denudation. At warmer temperatures, small and inefficient glaciers limit denudation. (C) The influence of temperature distribution on long-term changes in denduation following glaciation. Denudation rates are calculated for only the glaciated region (ice > 10 m) and are averaged for 2 My following the onset of glaciation. The percent change along the x-axis is relative to the preglacial, stedy-state denudation rate. Shapes denote different rock-uplift rates and color denotes baselevel temperature.

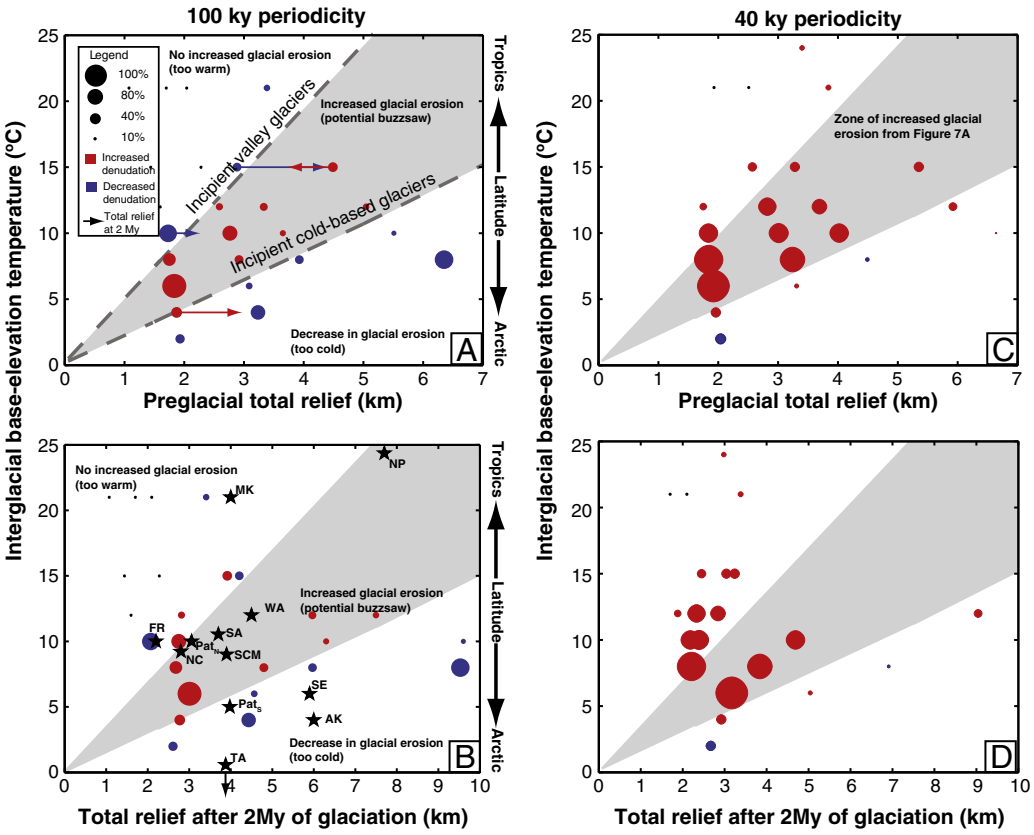

Fig. 7. The effects of climate and topography on the mode of glacial erosion for 100 ky periodicity in glacial–interglacial cycles (A). Interglacial baselevel temperature (sea-level for model scenarios) on the y-axis vs. total relief at the start of glaciation. Circles are modeled data and the size depends on the magnitude of change in average erosion rate in the glaciated region for the 2 Ma following glacial onset. Red denotes an increase in erosion, blue a decrease. Arrows denote change in relief for a few selected model runs after 2 My of glaciation. The shaded area defines a zone of increased erosion. Above this line erosion rates are slightly decreased with respect to non-glacial conditions. Well above this line, glaciers are not possible. Below the 'Buzzsaw' zone, cold-based glaciers dominate and erosion is reduced. (B) Same as (A), but x-axis is total relief after 2 My of glaciation. The majority of simulations show an increase in the total relief from glaciation. Black stars denote modern orogen baselevel temperatures and relief and coincide with locations of glaciated mountain ranges discussed in the text. (C) and (D) are same as (A) and (B) but for the 40 ky climate periodicity experiments.

to generate large valley glaciers but not too cold to be dominated by cold-based, unerosive ice. In Fig. 7B, model results are compared with temperature and relief data from glaciated orogens from around the world. This comparison is addressed in the discussion section.

3.5. Sensitivity of denudation rates to climate periodicity and erosional parameters

The previous results are sensitive to the choice of parameters used in the simulations. We conducted 51 simulations that evaluate the sensitivity of results to variations in the periodicity of glacial–interglacial cycles (Figs. 7C, D, and 8), glacial erosion efficiency (K_g), and fluvial erosion efficiency (K_f) (Figs. 8 and 9). It should be noted that glacial and fluvial erosional efficiency parameters are poorly constrained and our initial value used in the previous results is based on a handful of available studies (e.g. Humphrey and Raymond, 1994; Stock and Montgomery, 1999). Given this limitation, a sensitivity analysis of results to this parameter is warranted. We found results to be most sensitive to variations in glacial erosion efficiency and summarize the effects of this on denudation rates in the following

3.5.1. Sensitivity of denudation rates to climate periodicity

A similar pattern in increased and decreased denudation rates for variable base-elevation temperature and relief occurs with a climate periodicity of 40 ky (Fig. 7C, D) as the previously described 100 ky periodicity (Fig. 7A, B). However, the magnitude of increase or decrease in denudation rates varies with the climate periodicity. For example, using the same magnitude of glacial–interglacial temperature variation, the results from a 40 ky periodicity climate result in higher denudation rates following the onset of glaciation (compare light- and dark-blue bars, Fig. 8). This increase in denudation rates with a 40 ky periodicity is evident in a ~50% increase in denudation rates (red circles) shown Fig. 7C, D compared to Fig. 7A, B. Furthermore, regions with a decrease in denudation rates with a 100 ky periodicity (Fig. 7A, B) demonstrate a smaller decrease in denudation rates, or in some cases switch to an increase in denudation, with a 40 ky periodicity. Thus, a more pronounced difference in the effect of glacial denudation on landscapes is predicted with a climate periodicity of 40 ky.

The difference in denudation magnitudes between the 40 and 100 ky periodicities results from the differences in the initial (preglacial) fluvial and hillslope dominated topography. In all cases, the 40 ky landscape has slightly steeper slopes (~100 to 500 m more total relief) than the 100 ky scenario. This results from of a combination of (1) variable discharge produced by the temperature dependent orographic precipitation model and (2) the threshold incorporated in the linear sediment cover river erosion model (Braun and Sambridge, 1997). Essentially, the longer cycles (100 ky) exceed the erosion threshold (during warm and wet phases) for a longer period of time, and therefore, the 100 ky climate causes a more efficient fluvial erosion regime. The greater efficiency leads to lower river slopes and slightly less steep preglacial topography than

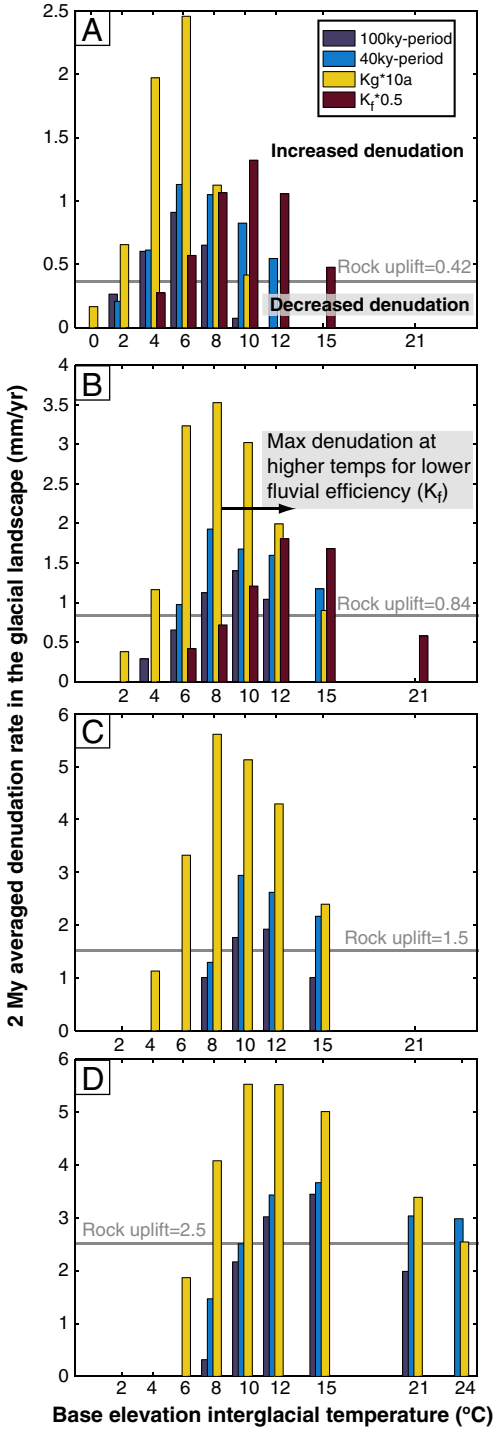

Fig. 8. Sensitivity of average denudation rate for the 2 My following the onset of glaciation for variations in climate and erosion parameters. Results are shown versus interglacial baselevel temperature used in simulations (sea-level in these simulations). Bar color represents model experiment. (A) is for rock-uplift of 0.42 mm/yr, (B) is for 0.84 mm/yr, (C) is for 1.5 mm/yr, and (D) is for 2.5 mm/yr. The thin gray line in each figure is the rate of rock-uplift. Bars extending above (below) this line represent scenarios in which an increase (decrease) in glacial landscape erosion occurs. The 40 ky experiments (light-blue bars) are generally more erosive than the 100 ky experiments (dark-blue). Increasing the glacial erosion coefficient (yellow bars) by 10-fold, increases the average denudation. Note the shift of the peak values in the red-bars at warmer temperatures in (A) and (B) is due to greater initial relief caused by the reducing fluvial erosional efficiency by one half.

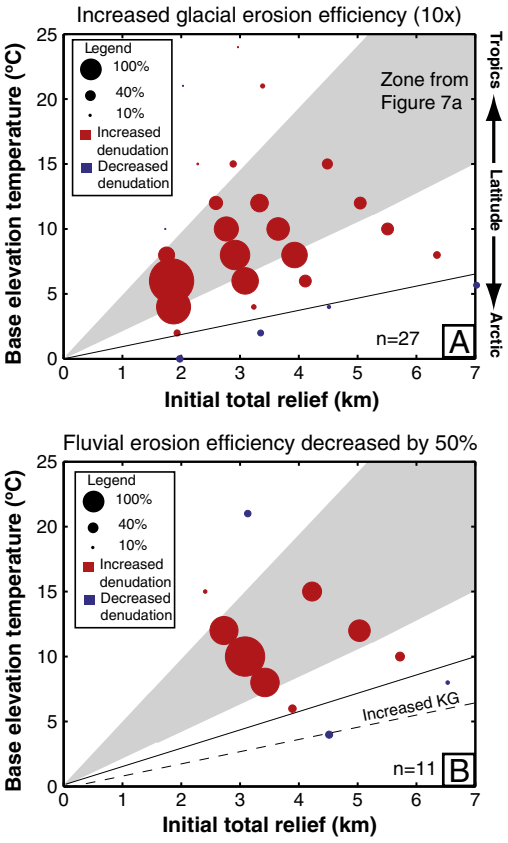

Fig. 9. Model sensitivity to (A) increased glacial erosion efficiency, K_g, by 10-fold and (B) decreased fluvial erosion efficiency, K_f by one half. Axes and symbols are the same as in Fig. 7. For both sensitivity tests, the lower (cooler) boundary for the transition (thin line) from increased denudation to decreased is lowered by 2–3 °C. Gray-area is the zone of increased denudation from Fig. 7A. Dashed line in (B) the thin line from (A).

the 40 ky cycles. When glaciers develop, they are slightly more erosive due to the steeper topography, causing more pronounced transience and higher average denudation rates.

3.5.2. Sensitivity of denudation rates to erosion parameters

Variations in the fluvial and glacial erosion parameters have a minor effect on the pattern of results shown in Figs. 6 and 7 but have a larger influence on the magnitude of change in glacial denudation rates (Fig. 8). The sensitivity of denudation rates to the selected glacial erosion coefficient, K_g, was evaluated by increasing the value 10-fold (to 10^{-3}). All results shown in Fig. 7 were then recomputed. An increase in K_g by an order of magnitude expands the zone of enhanced denudation (Fig. 9A) and lowers the threshold of decreased erosion by only ~2–3 °C. Furthermore, changes in the magnitude of denudation rates are amplified by an increase in K_g. For example, the highest relative change in erosion for values of K_g occurs at a rock-uplift rate of 0.42 mm/yr (at ~2 km relief) and a base level temperature of 6 °C (Figs. 7A and 8A). For this scenario, denudation is enhanced by ~485% (2.5 mm/yr) for 2 My following glacial onset (Figs. 8A and 9A), whereas a K_g of 10^{-4} experiences only a ~115% increase (0.9 mm/yr) (Figs. 7A and 8A).

A second test of the model sensitivity to erosional parameters was calculated by decreasing the fluvial erosion coefficient (K_f) by one half. We only explore the results with the two lowest rates of rock-uplift (0.42 and 0.84 mm/yr, Fig. 8A, B) because at higher uplift rates, variations in K_f lead to geologically unrealistic initial topography. In general, we found that lower fluvial erosion efficiency leads to higher initial topography, as expected from previous studies (Whipple and Tucker, 1999; Whipple et al., 1999). Because

topographic slopes are enhanced for a given rate of rock uplift with decreased fluvial erosion efficiency, changes in denudation with the onset of glaciers are slightly enhanced (Fig. 9B). Furthermore, the temperature range that causes an increase in erosion rates is shifted to warmer baselevel temperatures (red bars Fig. 8) because of the higher preglacial topography. The transition from increased denudation in the glaciated part of the landscape is lowered by only ~1 °C, with a maximum occurring for the lowest rock uplift rate and a baselevel temperature of 10 °C as erosion rates were increased from 0.42 mm/yr to 1.3 mm/yr (Figs. 8 and 9).

In summary, we find that variations in the glacial and fluvial erosional efficiency both influence the magnitude of denudation. Not surprisingly, increases in glacial erosional efficiency, K_g, will increase the average denudation of the glaciated landscape; however, the climatic window or temperature range that defines the zone of increased denudation is only affected by a few degrees, despite the order of magnitude change in glacial erosion efficiency. Changes in fluvial erosion efficiency, K_f, primarily influence denudation by altering the relief structure of the pre-glaciated orogen. Lowering the value shifts the window of increased denudation to warmer climates maintaining the general relationship amongst climate, relief, and changes in denudation. Given this, the results presented in Figs. 6 and 7 should be robust and broadly applicable to a wide range of geologic and climatic settings where natural variations in these efficiency metrics are within the range of values considered here.

4. Discussion

There are three implications of the previous results for understanding if glacial conditions are more or less erosive than preglacial conditions. These include: (1) the identification of three climate-defined erosional zones for glaciated landscapes (Fig. 7), (2) large spatial and temporal variations in denudation rates that result in pulses of glacial landscape evolution (Fig. 4), and (3) latitudinal variations in glacial denudation observed in some regions. A more detailed discussion of each of these points follows.

4.1. The influence of climate on glacial erosion

Over multiple glacial–interglacial cycles, glacial erosion is predicted to behave differently within each of the zones previously discussed in Fig. 7. For example, at the onset of ice accumulation, denudation may be minimal owing to small, slowly moving glaciers. A cooler climate will generate larger glaciers, increase basal sliding velocities and valley bottom denudation thereby steepening local hill slopes and enhancing ice thickness and sliding velocities through snow avalanching onto the glacier. This combination of processes constitute a positive feedback whereby once a glacier of sufficient size develops it produces more favorable conditions for increased erosion, so long-as between ~10–60% of the landscape remains below freezing during the interglacial (Figs. 6C and 7A). After large glaciers fill the main valleys, deep incision and enhanced denudation occurs across the entire glaciated landscape (e.g. Fig. 1). In an even cooler climate, many of the main valley glaciers as well as all of the headwater cirques and ridges become frozen to their bed. Glaciers then cease sliding, and denudation is reduced to below pre-glacial rates (Fig. 6B).

The model prediction that a 40 ky cycle is more erosive than a 100 ky cycle is a function of the different landscape morphologies present at the initiation of glaciation. We note that variations in the glacial–interglacial magnitude (i.e. the amplitude of temperature change) with periodicity were not considered. Variations in the amplitude of temperature change could have increased during the transition to 100 ky periods (Clark et al., 2006). An increase in magnitude would likely have a bigger impact on changes in denudation rates than the minor differences in topography that resulted in our experiments from variations in periodicity alone. For example, Valla et al. (2011) infer a greater ice thickness in the Alps from increased denudation rates calculated at the transition to 100 ky periodicity. If true, thicker ice at this transition would lead to enhanced sliding and denudation; however such effects need to be established on a case-by-case basis and are not considered here. Nevertheless, this exercise reveals the importance of the initial morphology. Initial morphology is a product of the pre-glacial erosion efficiency state and controls the landscape response at the onset of glaciation. This finding is further supported by the experiments with a lower fluvial efficiency (Fig. 9B) that show for a given rock-uplift rate, a higher rate of glacial denudation following the onset of glaciation is expected due to the initially steeper topography (Fig. 8A and B).

4.2. Temporal and spatial variations in denudation

Several lines of geologic evidence support the large temporal variations in glacial denudation indicated in Fig. 4. For example, in the southern Coast Mountains of B.C., studies have documented a pulse of denudation (Ehlers et al., 2006; Shuster et al., 2005) at approximately 1.8 Ma even though glaciers existed in this region well before this time (Denton and Armstrong, 1969). Furthermore, Koppes and Hallet (2006) showed that denudation rates from glaciated landscapes are highly sensitive to the timescale over which the rate is calculated. Both their data and the results presented here (Fig. 4) show that averaging over longer timescales tends to lead to progressively lower estimates of denudation rate.

Many previous studies have shown that glacial erosion increases local relief (Herman and Braun, 2008; Kessler et al., 2008; Tomkin and Braun, 2002), which requires spatially variable erosion rates (Herman and Braun, 2008). The results presented here are consistent with the tendency for valley erosion to outpace ridge erosion following glacial onset (Fig. 2B, C, and D). The pulse of increased valley erosion, however, does not require the landscape-wide average erosion rate to increase because it can be offset by the decrease in ridge erosion Fig. 2B. Therefore the spectacular relief often attributed to glacial erosion, may very well be partly the result of reduced denudation and surface uplift along ridgelines (Fig. 2B).

4.3. Latitudinal variation in glacial denudation

Predicted variations in increased or decreased glacial denudation were compared with 12 modern glaciated orogens spanning latitudes from the arctic to the tropics (Fig. 7B). Each orogen shown has a different present day relief. To calculate relief, we clip the 90 m STRM (Farr et al., 2007) dataset to include only incised mountainous topography (e.g. we ignore any piedmonts). We then calculate the cumulative distribution function and chose the 99th percentile of the elevation distribution as the total relief. This effectively finds the highest peaks in the landscape and provides a measure of total landscape relief (i.e. the base-level to peak elevation difference). For interglacial baselevel temperature, we calculate the average annual temperature from weather stations nearest the mountain baselevel (e.g. sea-level or the piedmont elevation) using data from the Global Historical Climate Network (Peterson and Vose, 1997).

From this comparison, we find that the observed spatial (latitudinal) distribution of glacial erosion in mountains also qualitatively supports the results shown in Fig. 7. The general trend observed is that regardless of the total relief, lower latitude orogens plot above or near the warm boundary of the zone of enhanced denudation (Fig. 7), mid-latitude orogens plot in the middle of the zone, and high latitude orogens plot below. Estimates of long-term denudation rates that are available for some of these orogens are consistent with the predicted patterns. For example, mountains at lower latitudes with only small glaciers during interglacial periods, such as the Front Range of Colorado, show little evidence of increased denudation

over long-time scales relative to pre-glacial conditions (Pazzaglia and Kelley, 1998). Such landscapes are predicted to be highly sensitive to continued global cooling and thus exhibit large spatial variability in denudation rates. The Front Range also supports this prediction as recent valley denudation has outpaced the low rates of sub-summit denudation by several orders of magnitude (Anderson, 2002; Small and Anderson, 1998). Upper mid-latitude ranges such as the western Alps and southern Coast Mountains, show clear evidence of enhanced denudation over the last 2–4 My (Ehlers et al., 2006; Valla et al., 2011; Vernon et al., 2008) and plot within or near the predicted zone of increased denudation (Fig. 7B). The Southern Alps of New Zealand also plot within this zone of increased denudation (Fig. 7B) and may appear at odds with a recent finding based on OSL thermochronology (Herman et al., 2010) that suggests a constant exhumation over glacial–interglacial cycles; however, this method is sensitive to only the last ~100 ky, whereas (U–Th)/He thermochronologic data that averages over many glacial cycles shows a transience in erosion rate over the last 2 My (Shuster et al., 2011).

Ranges located at high latitudes show evidence of a transition to lower denudation conditions (Fig. 7B, lower right zone). For example, the Trans Antarctic mountains were more erosive in earlier times when global climate was warmer (Miller et al., 2010; Sugden and Denton, 2004) but the cessation of erosion is coincident with the expansion of the Antarctic ice sheet in the mid-Miocene (Miller et al., 2010) (Fig. 7B, lower right zone). Thermochronometer data from the Alaska Range reveal an increase in denudation at ~5–6 Ma (Fitzgerald et al., 1993). The existence of Mount Denali (>6 km high), however, suggests that a glacial buzzsaw no longer limits topography in this area (Griffiths, 1952) since a MAT of <0 °C likely occurs at elevations less than 1 km for a baselevel temperature of 4 °C and a lapse rate of 6.5 °C/km (e.g. Fig. 3A). Although the St. Elias Range shows evidence of very high, localized denudation (Berger et al., 2008; Enkelmann et al., 2010), other parts of the range such as the Mt. Logan Massif and other areas of SE Alaska have experienced reduced rates of denudation (Enkelmann et al., 2010; Meigs and Sauber, 2000; Spotila and Berger, 2010). The results presented here, suggest the St. Elias range is very near the transition to landscapes dominated by cold-based glaciers in which average denudation rates across the landscape are lower than rates would be in the absence of glaciers.

Latitudinal dependent climate change in the Late Cenozoic (Robinson et al., 2008) is an additional consideration for the spatial control of glacial denudation histories. More rapid climate change at high latitudes, compared to lower latitudes, could have inhibited rapid denudation and enhanced the development of anomalously high topography (e.g. Mount Denali). More modest climate change at lower latitudes, such as the western Alps and the southern Coast Mountains, has allowed the sustainment of increased erosion throughout the Pleistocene. For example, high latitudes have cooled as much as 7 °C since ~3.3 Ma (Robinson et al., 2008). Given a lapse rate of ~6.5 °C/km, this equates to a suppression of the freezing line of ~330 m every 1 My. Mid-latitudes cooled about twice as slowly, providing these landscapes with more time to adjust to the cooling climate and maintain topography below the maximum ELA (Fig. 3).

5. Conclusion

The influence of climate and topography on the erosive nature of glacial conditions (e.g. a glacial 'buzzsaw') is a subject of ongoing scientific inquiry. Here we show how those parameters successfully predict the erosional state of a glaciated mountain range, and we have constrained the climatic bounds over which an increase in glacial erosion is expected for a given topography. Our work extends beyond the simple 'buzzsaw' hypothesis and predicts under what climate and tectonic (rock-uplift) conditions an increase or decrease in glacial denudation will occur. Furthermore, we find that the development of cold-based glaciers at high latitudes and high rates of tectonic uplift cause deviations from buzzsaw-like conditions and are probable in locations such as the southern Patagonia and Alaskan Range. Temporal variability in denudation rates is predicted over a range of timescales due to the evolution of glaciated topography. Local differences in erosion rate (e.g. between a valley and a ridge) can lead to the enhancement of local relief but with little change in landscape average erosion rate. Finally, spatial variations in the magnitude of Late Cenozoic climate change have caused significant latitudinal differences in the temporal evolution of denudation rates in glaciated mountains.

Acknowledgments

The authors are grateful to F. Herman and J. Braun for sharing the ICE and CASCADE source code that was modified for this study. W. Kappler is thanked for assistance in model coupling and program modification. G. Roe is thanked for discussions and source code related to the orographic model used in this study. This work was funded by the US National Science Foundation and German National Science Foundation grants to T. Ehlers (NSF-0724656; DFG-EH 329/1-1). D. Burbank and F. Herman are thanked for constructive and thorough reviews.

Appendix A. Supplementary data

Supplementary data to this article can be found online at doi:10.1016/j.epsl.2012.01.030.

References

Anderson, R.S., 2002. Modeling the tor-dotted crests, bedrock edges, and parabolic profiles of high alpine surfaces of the Wind River Range, Wyoming. Geomorphology 46, 35–58.
Bartholomaus, T.C., Anderson, R.S., Anderson, S.P., 2008. Response of glacier basal motion to transient water storage. Nat. Geosci. 1, 33–37.
Berger, A.L., Gulick, S.P.S., Spotila, J.A., Upton, P., Jaeger, J.M., Chapman, J.B., Worthington, L.A., Pavlis, T.L., Ridgway, K.D., Willems, B.A., McAleer, R.J., 2008. Quaternary tectonic response to intensified glacial erosion in an orogenic wedge. Nat. Geosci. 1, 793–799.
Braithwaite, R.J., 1995. Positive degree-day factors for ablation on the Greenland ice sheet studied by energy-balance modelling. J. Glaciol. 41, 153–160.
Braun, J., Sambridge, M., 1997. Modelling landscape evolution on geological time scales: a new method based on irregular spatial discretization. Basin Res. 9, 27–52.
Braun, J., Zwartz, D., Tomkin, J., 1999. A new surface-processes model combining glacial and fluvial erosion. Ann. Glaciol. 28, 282–290.
Brocklehurst, S.H., Whipple, K.X., 2002. Glacial erosion and relief production in the Eastern Sierra Nevada, California. Geomorphology 42, 1–24.
Broecker, W.S., Denton, G.H., 1989. The role of ocean–atmosphere reorganizations in glacial cycles. Geochim. Cosmochim. Acta 53, 2465–2501.
Brozović, N., Burbank, D.W., Meigs, A.J., 1997. Climatic limits on landscape development in the Northwestern Himalaya. Science 276, 571–574.
Burbank, D.W., Leland, J., Fielding, E., Anderson, R.S., Brozovic, N., Reid, M.R., Duncan, C., 1996. Bedrock incision, rock uplift and threshold hillslopes in the northwestern Himalayas. Nature 379, 505–510.
Clark, P.U., Archer, D., Pollard, D., Blum, J.D., Rial, J.A., Brovkin, V., Mix, A.C., Pisias, N.G., Roy, M., 2006. The middle Pleistocene transition: characteristics, mechanisms, and implications for long-term changes in atmospheric pCO_2. Quat. Sci. Rev. 25, 3150–3184.
Densmore, M.S., Ehlers, T.A., Woodsworth, G., 2007. Effect of Alpine glaciation on thermochronometer age-elevation profiles. Geophys. Res. Lett. 34.
Denton, G.H., Armstrong, R.L., 1969. Miocene–Pliocene glaciations in southern Alaska. Am. J. Sci. 267, 1121–1142.
Egholm, D.L., Nielsen, S.B., Pedersen, V.K., Lesemann, J.-E., 2009. Glacial effects limiting mountain height. Nature 460, 884–887.
Ehlers, T.A., Farley, K.A., Rusmore, M.E., Woodsworth, G.J., 2006. Apatite (U–Th)/He signal of large-magnitude accelerated glacial erosion, southwest British Columbia. Geology 34, 765.
Enkelmann, E., Zeitler, P.K., Garver, J.I., Pavlis, T.L., Hooks, B.P., 2010. The thermochronological record of tectonic and surface process interaction at the Yakutat–North American collision zone in southeast Alaska. Am. J. Sci. 310, 231–260.
Farr, T.G., Rosen, P.A., Caro, E., Crippen, R., Duren, R., Hensley, S., Kobrick, M., Paller, M., Rodriguez, E., Roth, L., Seal, D., Shaffer, S., Shimada, J., Umland, J., Werner, M., Oskin, M., Burbank, D., Alsdorf, D., 2007. The shuttle radar topography mission. Rev. Geophys. 45 33 PP.
Fitzgerald, P.G., Stump, E., Redfield, T.F., 1993. Late Cenozoic uplift of Denali and its relation to relative plate motion and fault morphology. Science 259, 497–499.

Flowers, G.E., Clarke, G.K.C., 2002. A multicomponent coupled model of glacier hydrology 1. Theory and synthetic examples. J. Geophys. Res. 107 17 PP.
Griffiths, T.M., 1952. Glacial Geomorphology on the Mt. McKinley Massif, Alaska. Proceedings, Eighth General Assembly and Seventeenth International Congress. International Geographical Union, D. Washington, pp. 331–336.
Hallet, B., Hunter, L., Bogen, J., 1996. Rates of erosion and sediment evacuation by glaciers: a review of field data and their implications. Glob. Planet. Chang. 12 (1–4), 213–235.
Herman, F., Braun, J., 2008. Evolution of the glacial landscape of the Southern Alps of New Zealand: insights from a glacial erosion model. J. Geophys. Res. 113.
Herman, F., Rhodes, E.J., Braun, J., Heiniger, L., 2010. Uniform erosion rates and relief amplitude during glacial cycles in the Southern Alps of New Zealand, as revealed from OSL-thermochronology. Earth Planet. Sci. Lett. 297, 183–189.
Herman, F., Beaud, F., Champagnac, J.-D., Lemieux, J.-M., Sternai, P., 2011. Glacial hydrology and erosion patterns: a mechanism for carving glacial valleys. Earth Planet. Sci. Lett. 310, 498–508.
Humphrey, N.F., Raymond, C.F., 1994. Hydrology, Erosion and Sediment Production in a Surging Glacier: Variegated Glacier, Alaska, 1982–83.
Kamb, B., 1987. Glacier Surge Mechanism Based on Linked Cavity Configuration of the Basal Water Conduit System.
Kessler, M., Anderson, R., Stock, G., 2006. Modeling topographic and climatic control of east-west asymmetry in Sierra Nevada glacier length during the Last Glacial Maximum. J. Geophys. Res. 111, no. F2.
Kessler, M., Anderson, R., Briner, J., 2008. Fjord insertion into continental margins driven by topographic steering of ice. Nat. Geosci. 1, 365–369.
Koppes, M., Hallet, B., 2006. Erosion rates during rapid deglaciation in Icy Bay, Alaska. J. Geophys. Res. Earth Surf. 111, 02023.
Koppes, M.N., Montgomery, D.R., 2009. The relative efficacy of fluvial and glacial erosion over modern to orogenic timescales. Nat. Geosci. 2, 644–647.
MacGregor, K.R., Anderson, R.S., Anderson, S.P., Waddington, E.D., 2000. Numerical simulations of glacial-valley longitudinal profile evolution. Geology 28, 1031.
Meigs, A., Sauber, J., 2000. Southern Alaska as an example of the long-term consequences of mountain building under the influence of glaciers. Quat. Sci. Rev. 19, 1543–1562.
Miller, S.R., Fitzgerald, P.G., Baldwin, S.L., 2010. Cenozoic range-front faulting and development of the Transantarctic Mountains near Cape Surprise, Antarctica: thermochronologic and geomorphologic constraints. Tectonics 29.
Mitchell, S., Montgomery, D., 2006. Influence of a glacial buzzsaw on the height and morphology of the Cascade Range in central Washington State, USA. Quat. Res. 65, 96–107.
Paterson, W.S.B., 1994. The physics of glaciers. Butterworth-Heinemann.
Pazzaglia, F.J., Kelley, S.A., 1998. Large-scale geomorphology and fission-track thermochronology in topographic and exhumation reconstructions of the Southern Rocky Mountains. Rocky Mt. Geol. 33, 229–257.
Pelletier, J.D., Comeau, D., Kargel, J., 2010. Controls of glacial valley spacing on earth and mars. Geomorphology 116, 189–201.
Penck, A., 1905. Glacial features in the surface of the Alps. J. Geol. 13, 1–19.
Peterson, T.C., Vose, R.S., 1997. An overview of the global historical climatology network temperature database. Bull. Am. Meteorol. Soc. 78, 2837–2849.
Porter, S.C., 1989. Some geological implications of average Quaternary glacial conditions. Quat. Res. 32, 245–261.
Robinson, M.M., Dowsett, H.J., Chandler, M.A., 2008. Pliocene role in assessing future climate impacts. Eos Trans. Am. Geophys. Union 89, 501.
Roe, G.H., Montgomery, D.R., Hallet, B., 2003. Orographic precipitation and the relief of mountain ranges. J. Geophys. Res. 108 12 PP.
Shuster, D.L., Ehlers, T.A., Rusmoren, M.E., Farley, K.A., 2005. Rapid glacial erosion at 1.8 Ma revealed by $^{4}He/^{3}He$ thermochronometry. Science 310, 1668–1670.
Shuster, D.L., Cuffey, K.M., Sanders, J.W., Balco, G., 2011. Thermochronometry reveals headward propagation of erosion in an Alpine landscape. Science 332, 84–88.
Small, E.E., Anderson, R.S., 1998. Pleistocene relief production in Laramide mountain ranges, western United States. Geology 26, 123.
Spotila, J.A., Berger, A.L., 2010. Exhumation at orogenic indentor corners under long-term glacial conditions: example of the St. Elias orogen, Southern Alaska. Tectonophysics 490, 241–256.
Stock, J.D., Montgomery, D.R., 1999. Geologic constraints on bedrock river incision using the stream power law. J. Geophys. Res. 104, 4983–4993.
Stolar, D., Roe, G., Willett, S., 2007. Controls on the patterns of topography and erosion rate in a critical orogen. J. Geophys. Res. 112 17 PP.
Sugden, D., Denton, G., 2004. Cenozoic landscape evolution of the Convoy Range to Mackay Glacier area, Transantarctic Mountains: onshore to offshore synthesis. Geol. Soc. America. Bull. 116, 840.
Thomson, S.N., Brandon, M.T., Tomkin, J.H., Reiners, P.W., Vasquez, C., Wilson, N.J., 2010. Glaciation as a destructive and constructive control on mountain building. Nature 467, 313–317.
Tomkin, J.H., Braun, J., 2002. The influence of alpine glaciation on the relief of tectonically active mountain belts. Am. J. Sci. 302, 169–190.
Valla, P.G., Shuster, D.L., van der Beek, P.A., 2011. Significant increase in relief of the European Alps during mid-Pleistocene glaciations. Nat. Geosci. 4, 688–692.
Vernon, A.J., van der Beek, P.A., Sinclair, H.D., Rahn, M.K., 2008. Increase in late Neogene denudation of the European Alps confirmed by analysis of a fission-track thermochronology database. Earth Planet. Sci. Lett. 270, 316–329.
Whipple, K.X., Tucker, G.E., 1999. Dynamics of the stream-power river incision model: implications for height limits of mountain ranges, landscape response timescales, and research needs. J. Geophys. Res. 104, 17,661–17,674.
Whipple, K.X., Kirby, E., Brocklehurst, S.H., 1999. Geomorphic limits to climate-induced increases in topographic relief. Nature 401, 39–43.